PAPER

Nanofluidic charged-coupled devices for controlled DNA transport and separation

IOP Publishing Nanotechnology
Nanotechnology 32 (2021) 345501 (8pp) https://doi.org/10.1088/1361-6528/ac027f

Nanofluidic charged-coupled devices for controlled DNA transport and separation

Reza Nouri[1] **and Weihua Guan**[1,2]

[1] Department of Electrical Engineering, Pennsylvania State University, University Park, PA 16802, United States of America
[2] Department of Biomedical Engineering, Pennsylvania State University, University Park, PA 16802, United States of America

E-mail: w.guan@psu.edu

Received 1 February 2021, revised 10 May 2021
Accepted for publication 18 May 2021
Published 3 June 2021

Abstract

Controlled molecular transport and separation is of significant importance in various applications. In this work, we presented a novel concept of nanofluidic molecular charge-coupled device (CCD) for controlled DNA transport and separation. By leveraging the unique field-effect coupling in nanofluidic systems, the nanofluidic molecular CCD aims to store charged biomolecules such as DNAs in discrete regions in nanochannels and transfer and separate these biomolecules as a charge packet in a bucket brigade fashion. We developed a quantitative model to capture the impact of nanochannel surface charge, gating voltage and frequency, molecule diffusivity, and gating electrode geometry on the transport and separation efficiency. We studied the synergistic effects of these factors to guide the device design and optimize the DNA transport and separation in a nanofluidic CCD. The findings in this study provided insight into the rational design and implementation of the nanofluidic molecular CCD.

Supplementary material for this article is available online

Keywords: nanofluidics, charge-coupled device, molecular transport, molecular separation

(Some figures may appear in colour only in the online journal)

1. Introduction

The ionic and molecular transport phenomena in nanoscale channels are much different from those in larger micrometer- and millimeter-scale structures [1–3]. These differences stem from the unique characteristics of nanoscale structures, such as enhanced surface-to-volume ratios, and comparability of nanochannel size to the Debye length in ionic solutions [4, 5]. Over the past decade, these unique characteristics have been leveraged for developing many different nanofluidic devices such as diode [6–8], bipolar junction transistor [9, 10], field-effect transistor (FET) [11–19], and energy harvesting device [20–22]. Among these devices, voltage-gated ionic and molecular transport is the most intriguing [23]. It borrows inspiration from its solid-state counterparts, such as metal oxide semiconductor field-effect transistor (MOSFET). Similar to electrons/holes being modulated in the MOSFET device by an external electric field, the cation/anion (positively/negatively charged molecule) population in the nanochannels can be manipulated in a similar fashion in a nanofluidic FET. Active modulation of ions and molecules via field-effect gating in nanofluidic channels is attractive for various applications since it offers a unique opportunity to integrate wet ionics with dry electronics. So far, the direct electric field-charge interaction in nanochannels has been used for regulating the ion [24–28], protein [14], DNA [29], and fluid [30] transport. For instance, Paik *et al* utilized an array of electrically gated ~200 nm solid-state pores as nanofluidic transistors to manipulate the capture of DNA molecules [29]. In another study, Liu *et al* reduced the DNA translocation speed across a nanochannel by modulating the channel surface charge through an externally applied gate bias [18].

The solid-state charge-coupled device (CCD), building with an array of metal-oxide-semiconductor capacitors, is now widely used as the image sensor. The seminal work describing the CCD concept envisioned that the device could be used as a memory, a delay line, an imaging device, and a shift register

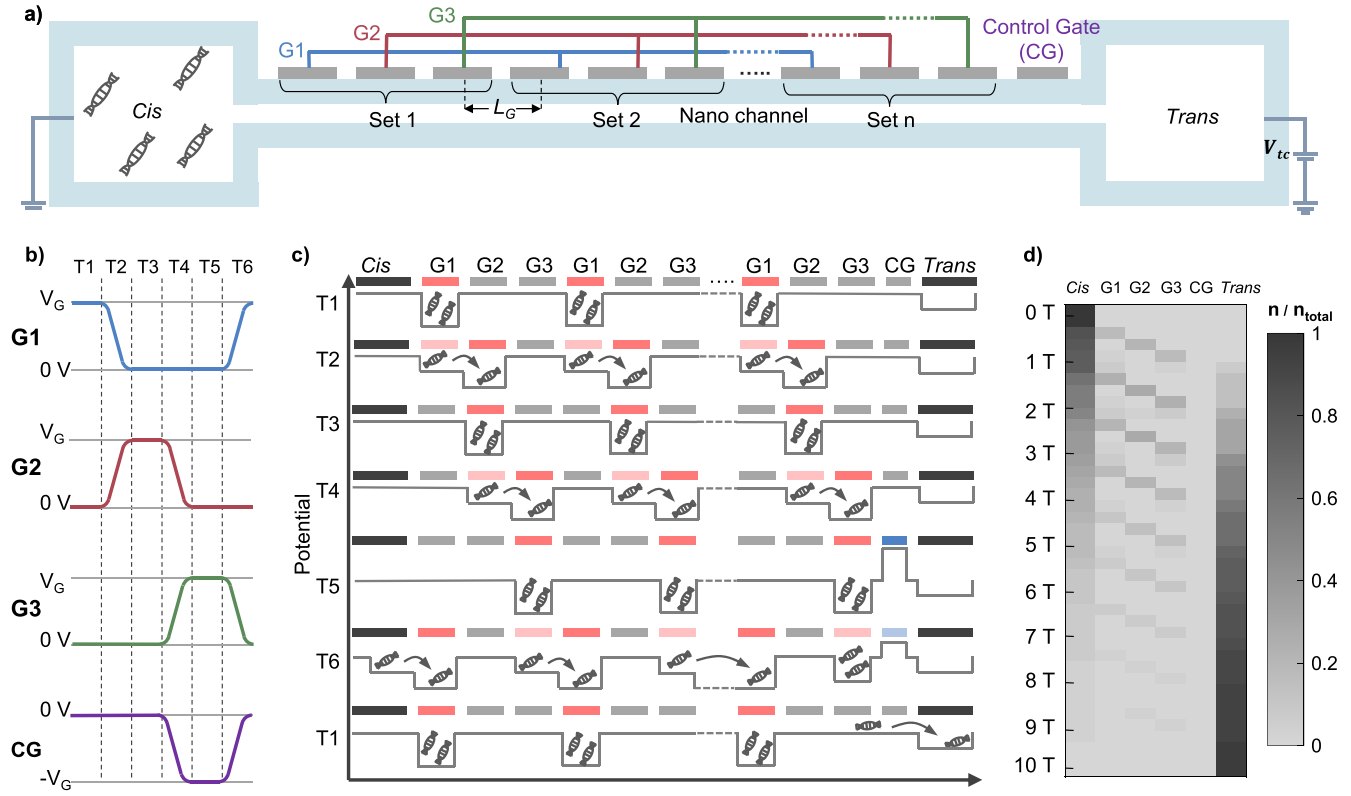

Figure 1. Overview of the nanofluidic charge-coupled device (CCD). (a) Schematic layout for nanofluidic CCD and its enlarged nanofluidic channel with multiple gate structures. (b) A three-phase clocking scheme for gate electrodes. T1–T6 are different time spots. (c) Illustrative distribution of DNAs under a clocking gate voltage at different time spots (T1–T6). (d) Simulation results of DNA transport through the nanofluidic molecular CCD with one set of gates. The diffusivity of the DNA is 2×10^{-12} m^2 s^{-1}. A 1.5 V voltage with a frequency of 0.1 Hz was applied to the gates. The gate electrode pitch size is 4.5 μm. The surface charge of the nanochannel is -2 mC m^{-2}. V_{tc} of 50 mV was applied across the channel.

[31]. CCDs store charges in discrete regions in a semiconductor and transfer the charges as a packet in a bucket brigade fashion [31]. Based on the field-effect coupling in nanofluidic devices, Stern *et al* conceptually proposed a sensitive chemical sensor (chemical ionic CCD) with a theoretically predicted ionic detection limit $<1 \times 10^{-13}$ M [28]. It was an extension of the single-gate ionic FET to multiple-gate structures. It was expected to have the capability of concentrating ions for sensitive detection. While biomolecules manipulation such as DNAs has been achieved by electric field-charge interaction in nanochannels [18, 29], the conceptual CCD mechanism for a bucket brigade transport of charged biomolecules has not been explored in a nanofluidic device.

In this work, we explored the CCD concept for controlled molecular transport and separation, fundamentally different from the conventional passive gel and capillary methods [32, 33]. We numerically studied the transport and separation efficiency in a three-phase nanofluidic molecular CCD. The effects of the nanochannel surface charge, gating voltage and clocking frequency, and molecular diffusion coefficient on the transport efficiency were elucidated. We also explored the feasibility of the nanofluidic molecular CCD for separating the DNA molecules based on their different diffusivities. We believe the proposed nanofluidic molecular CCD concept would open a new avenue for nanofluidic device research and offer a promising approach towards actively-controlled biomolecule transport and separation.

2. Device principle and modeling

2.1. Nanofluidic molecular CCD principles

The schematic layout for the nanofluidic molecular CCD and its enlarged nanofluidic channel with multiple gate structures is illustrated in figure 1(a). It consists of a long nanochannel in between two chambers: *cis* (reservoir chamber) and *trans* (outlet chamber). Two electrodes are placed in the chambers for applying the driving voltage V_{tc}. An array of gate electrodes with a fixed pitch size (L_G) is placed above the nanochannel with a three-phased biasing design (every three gating electrodes form a set). An output control gate (CG) is adopted immediately before the *trans* chamber to prevent the molecules from flowing back into the nanochannel. The analyte molecules are initially added into the *cis* chamber. Figure 1(b) shows the three-phase clocking scheme for gate electrodes (G1–G3) and the CG. Each clocking cycle can be divided into six distinct periods (T1–T6). Figure 1(c) illustrates the distribution of the DNA molecules at each of these different time spots. At the time of T1, a positive bias V_G is applied to each set's first gate electrode, which forms a packet

of negatively charged DNAs under that electrode. By positively biasing the consecutive electrodes, DNA packets can be moved through the nanochannel sequentially (T2–T5). The molecular flux through the nanochannel is the outcome of diffusion and drift forces. At the time of T6, a negative voltage ($-V_G$) is applied to the CG to prevent the molecules' backflow into the nanochannel. This process is periodically repeated. In each cycle, a portion of the molecules in the *cis* chamber will be transferred to the *trans* outlet. This working principle is very much like that in the solid-state CCD [31].

2.2. Device modeling

Diffusion and electrophoresis are the two mechanisms that determine the molecular translocation through the nanofluidic molecular CCD. To capture the DNA translocation, we need to compute these two motions. The Poisson–Nernst–Planck equations were used to capture the time-varying electric field, ionic, and molecules concentration as follows:

$$\nabla^2 V(t) = -\rho_e(t)/\varepsilon_0\varepsilon_r \tag{1}$$

$$\frac{\partial c_i(t)}{\partial t} + \nabla \cdot J_i(t) = 0 \tag{2}$$

in which $V(t)$ is the electric potential, and $\rho_e(t) = eN_A(\sum_i z_i c_i(t))$ is the charge density of mobile ions. ε_0, and ε_r are the vacuum and relative permittivity, respectively. Note that the molecules' charge density was not considered for calculating the potential distribution since their concentration (∼nM) is often negligible compared to that of ions (∼mM). In addition, the intermolecular interaction was not taken into consideration. The time-varying molecular and ionic flux density J_i (t) is given by:

$$J_i(t) = -D_i\nabla c_i(t) - c_i(t)(z_i\mu_i\nabla V(t)), \tag{3}$$

where D_i, μ_i z_i and c_i are the diffusivity, mobility, valance, and concentration of each species (ions and molecules). Electrophoretic mobility of DNAs after exceeding a certain length (∼100 bp) is identical. In this study, we did not consider shorter DNAs and fixed the electrophoretic mobility of the molecules as 4×10^{-8} $m^2\,V^{-1}.s^{-1}$.

The coupled mathematical model was numerically solved by COMSOL Multiphysics. A two-dimensional computational domain was developed based on the nanofluidic molecular CCD concept, and suitable boundary conditions were applied to capture the transient operation of the nanofluidic molecular CCD (supplementary figure S1 and table S1 (available online at stacks.iop.org/NANO/32/345501/mmedia)). In addition, supplementary note S1 presents the model details in terms of grid size and quality and convergence criteria.

3. Results and discussion

3.1. Controlled DNA transport in nanofluidic CCD

To illustrate the transient transport and the distribution of the molecules in each time segment, we simulated the transfer of DNAs with a typical diffusivity [34] of 2×10^{-12} m^2 s^{-1} through one set of nanofluidic molecular CCD for 10 cycles. Figure 1(d) shows the distribution of the molecules across the channel at different cycles. At each time spot, the number of molecules across the channel was normalized by the total number of starting molecules (n/n_{total}). At the beginning (0 T), all the molecules are at the *cis* (n_{cis} $/n_{\text{total}} = 1$). As the gating voltage cycles, the movement of DNA packets from the left (*cis*) to the right (*trans*) can be clearly observed. A discrete portion of the molecules was transferred to the *trans* chamber at the end of each cycle when the CG switched from $-V_G$ to 0 V. As the cycling continues, the transferred DNA molecules to the *trans* chamber were decreased. This is due to the fact that the difference between the *cis* and *trans* molecular concentration is reducing as the cycles continue, and consequently, the diffusion term of the molecular flux decreases. After about 10 cycles in this one set CCD, DNAs in the *cis* were almost entirely transferred to the *trans*.

3.2. Impact of surface charge on the transfer efficiency

It is well known that the nanochannel surface charges will significantly affect the electrokinetic transport of ions, fluids, and molecules in nanofluidic devices due to the effect of the electrical double layer [35, 36]. To study the effect of surface charge on the transport process in a CCD, we defined the transfer efficiency as the number of transported molecules to the *trans* as a percentage of the total number of molecules ($\eta = n_{trans}/n_{\text{total}}$). We studied the transfer efficiency of DNAs with a fixed diffusivity (2×10^{-12} m^2 s^{-1}) and gating voltage (1.2 V) for 100 cycles at different surface charges. In this study, we examined the device with one set of gates (three gates and one CG). The gating frequency was set at 0.1 Hz, and a lateral driving voltage V_{tc} of 50 mV was applied between *cis* and *trans*. Figure 2(a) shows the transfer efficiency as the function of time. We observed that the transfer efficiency was decreased as we increase the negative surface charge magnitude for a fixed operation time. This stems from the fact that the induced electric field by the negative surface charge and gating electrodes have opposite directions. The more negative surface charge we have, the more opposing forces will be applied to the negatively charged DNA molecules. The nanofluidic CCD will thus have less transfer efficiency. A neutral nanochannel surface charge is preferred towards higher transfer efficiency [37–39]. It should be noted that the transfer efficiency was not continuously increased as the operation time went by. This happened because only a discrete portion of the molecules was transferred to the *trans* chamber at the end of each cycle.

3.3. Impact of gating voltage magnitude on the transfer efficiency

The gating voltage not only alters the transverse electric field distribution in the nanochannel due to the double layer effect [40] but also impacts the lateral electric field and thus the electrophoretic force. Consequently, varying the gating voltage magnitude would have an impact on the molecular flux and transfer efficiency.

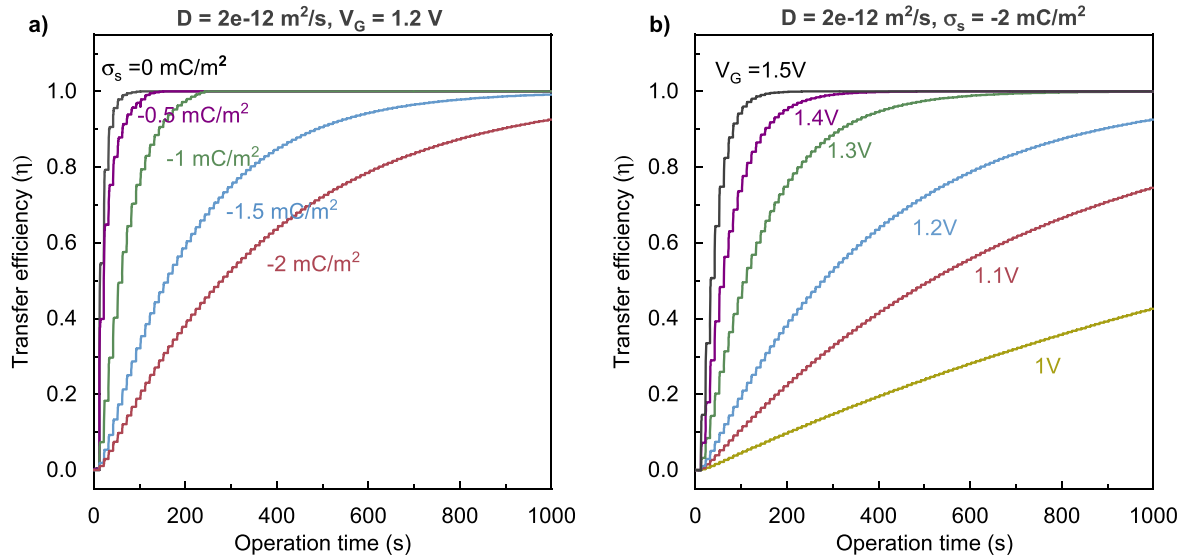

Figure 2. (a) Transfer efficiency of DNA with diffusivity of 2×10^{-12} m^2 s^{-1} at different surface charges for 1000 s. A gating voltage of 1.2 V at the frequency of 0.1 Hz was applied, and a lateral driving voltage V_{tc} of 50 mV was set between *cis* and *trans*. In all cases, we set up the simulation in one set of gates (three gates and one control gate). (b) Transfer efficiency of DNA with diffusivity of 2×10^{-12} m^2 s^{-1} at different gating voltages for 1000 s. The frequency was fixed at 0.1 Hz, and $V_{tc} = 50$ mV was applied across the channel. In all cases, the surface charge of -2 mC m^{-2} was used at nanochannel walls.

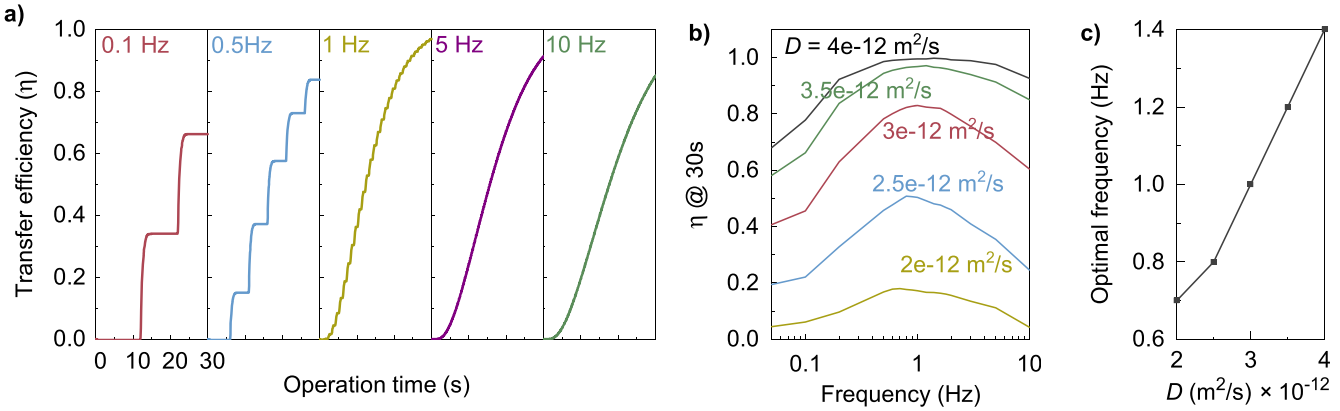

Figure 3. (a) Transfer efficiencies versus operation time at different frequencies (0.1, 0.2, 1, 5, 10 Hz). In all cases, the diffusivity and voltage were fixed at 3.5×10^{-12} m^2 s^{-1} and 1.3 V, respectively. $V_{tc} = 50$ mV was applied across the channel to reduce the effect of the surface charge. (b) Transfer efficiency of DNA with distinct diffusivities at a fixed gating voltage (1.3 V), and different frequencies. In all cases, the surface charge was fixed at -2 mC m^{-2}, and $V_{tc} = 50$ mV was applied across the channel. (c) Optimal frequency as a function of molecular diffusivity.

To capture the effect of gating voltage magnitude, we studied the transfer efficiency of DNAs with a fixed diffusivity (2×10^{-12} m^2 s^{-1}) at different gating voltages for 100 cycles. In all these cases, we selected the gating frequency at 0.1 Hz, the surface charge of the nanochannel at -2 mC m^{-2}, and lateral driving voltage V_{tc} as 50 mV. Figure 2(b) shows the transfer efficiency as the function of time. The transfer efficiency improved with increasing the gating voltages. This is not surprising since a larger gating voltage would create a higher lateral electric field, ∇V, and thus a higher electrophoretic flux ($\mu c\ \nabla V$).

3.4. Impact of clocking frequency and molecular diffusivity on the transfer efficiency

While gating voltage magnitude impacts the electrophoretic force's magnitude, gate clocking frequency would affect the transient dynamics of this force. To study the effect of the gating frequency on the transfer dynamics, we studied the transfer efficiency of DNAs with a fixed diffusivity (3.5×10^{-12} m^2 s^{-1}) and gating voltage (1.3 V) at different frequencies. Figure 3(a) shows the transfer efficiency as a function of time under various gating frequency scenarios. The transfer efficiency was improved when the frequency was increased from 0.1 to 1 Hz. However, increasing the frequency from 1 to 10 Hz reduced the transfer efficiency. This could be understood by the comparison between the clocking period ($\sim 1/f$) and the time for a given molecule to diffuse to the adjacent electrode ($\sim L_G^2/D$). If the clocking occurs too fast ($1/f \ll L_G^2/D$), some of the molecules in each packet will be left behind and later localized in a trailing packet, reducing the transfer efficiency.

Since the impact of the molecule diffusivity on the transfer dynamic depends on the gating frequency, we set out

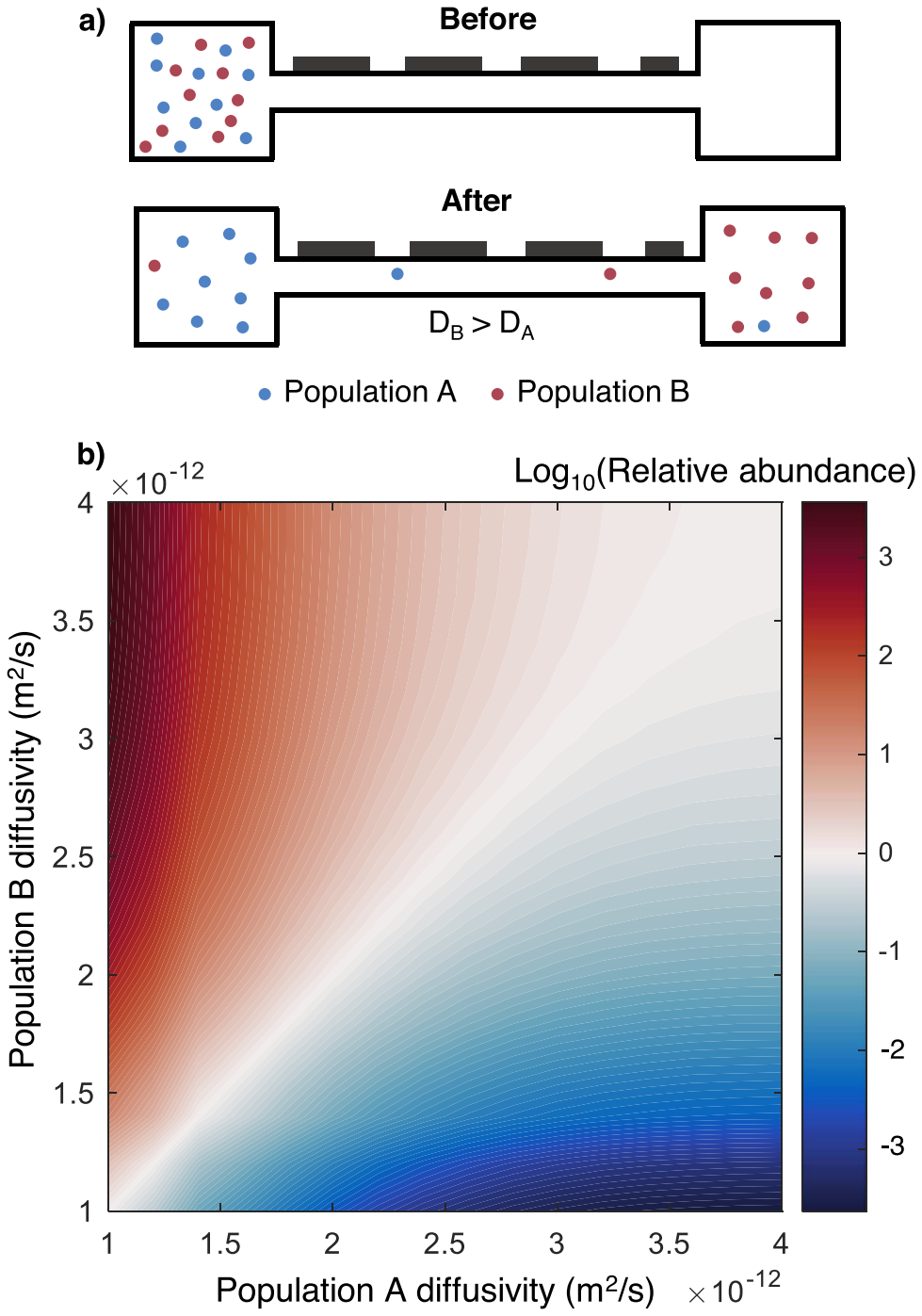

Figure 4. (a) Schematic of the nanofluidic CCD separation, where two samples can be separated based on their diffusivities. (b) The relative abundance of two populations based on their diffusivities (1×10^{-12}–4×10^{-12} m^2 s^{-1}) after 50 s. In all cases, a fixed gating voltage of 1.2 V with a frequency of 0.1 Hz was applied, and $V_{tc} = 50$ mV was considered across the channel.

to study the effect of the molecule diffusivity on the transfer efficiency at different clocking frequencies. We studied the transfer efficiency of molecules with different diffusivities (2×10^{-12}–4×10^{-12} m^2 s^{-1}) and a fixed gating voltage of 1.3 V at various frequencies. Figure 3(b) illustrates the transfer efficiency as a function of clocking frequency at different diffusivities. We observed two features. One is that the transfer efficiency was always improved by increasing the molecule diffusivity (D) at a fixed clocking frequency. This is not surprising since increasing the molecule diffusivity would increase the diffusion term of the molecular flux ($D\nabla c$). The other feature was that for a fixed molecular diffusivity, the transfer efficiency went up with increasing the frequency until reaching a peak, after which the transfer efficiency reduced when further increasing the frequency. We defined the frequency at which the transfer efficiency was maximized as optimal frequency. Figure 3(c) presents the optimal frequencies as a function of DNA diffusivities. It is clear that the optimized clocking frequency goes

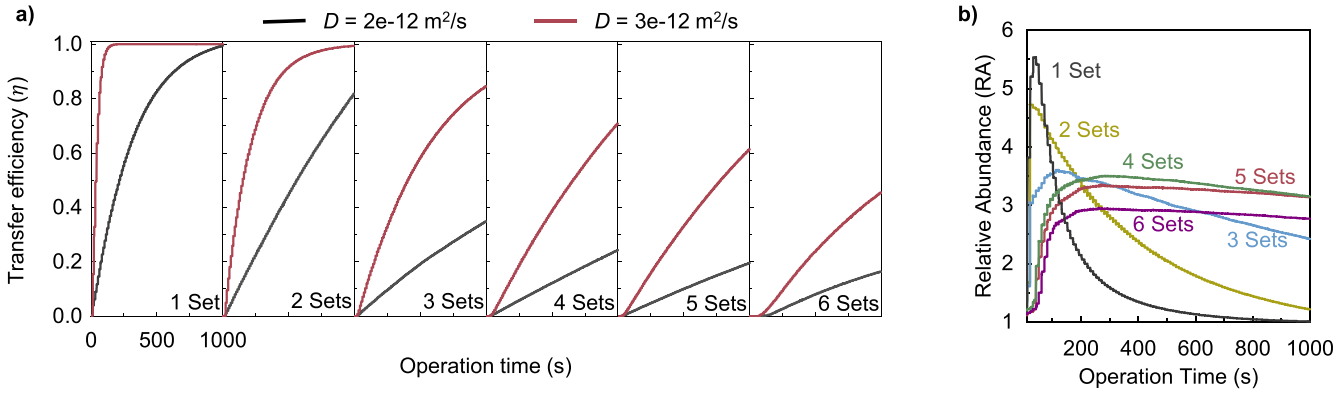

Figure 5. (a) Transfer efficiencies of the two populations with different diffusivities (2×10^{-12} and 3×10^{-12} m^2 s^{-1}) through the nanofluidic molecular CCD with a different number of sets (1–6) over 1000 s (100 cycles). In all cases, we applied a voltage of 1.2 V with a frequency of 0.1 Hz. (b) The relative abundance of the two populations through the nanofluidic molecular CCD with a different number of sets over 1000 s (100 cycles). In all cases, we applied a voltage of 1.2 V with a frequency of 0.1 Hz.

up when increasing the DNA diffusivities. This is due to the fact that the maximal transfer efficiency will happen when the clocking period matches the time required for the molecules to diffuse to the next electrode ($1/f \sim L_G^2/D$).

3.5. Use of nanofluidic CCD for diffusivity-based separation

Since the transfer efficiency strongly depends on the molecule diffusivities, nanofluidic CCD can be implemented for molecular separation based on their diffusivities. Figure 4(a) illustrates the schematic of nanofluidic CCD utilization for separating a mixed DNA sample consisting of two subpopulations *A* and *B*. Assuming population *B* has a higher diffusivity than *A*, more molecules *B* would be transferred to the *trans* outlet after operating the nanofluidic CCD for a particular time. As a result, we would be able to separate two subpopulations in a nanofluidic CCD. To quantify the separation efficiency, we defined the relative abundance (RA) of population *A* and *B* as $\frac{n_{A,\,trans}\,/\,n_{B,\,trans}}{n_{A,\,\mathrm{total}}\,/\,n_{B,\,\mathrm{total}}}$, in which $n_{A,\,\mathrm{total}}$ and $n_{B,\,\mathrm{total}}$ are the total number of molecules *A* and *B* respectively, $n_{A,\,trans}$ and $n_{B,\,trans}$ are the number of molecules *A* and *B* in the *trans* after a certain operation time.

Figure 4(b) shows the RA of population *A* and *B* at different combinations of diffusivities after 50 s of operation. A fixed gating voltage of 1.2 V with a frequency of 0.1 Hz was applied, and $V_{tc} = 50$ mV was considered across the channel. Not surprisingly, for cases where the diffusivities of the two populations are similar (the diagonal), we were not able to separate the samples (RA = 1). For cases where diffusivity of population *B* was larger than sample *A*, RA was larger than 1 which means we can separate population *B* from population *A*. At a constant diffusivity for population *A*, as we increased the diffusivity of population *B*, higher RA was achieved. In an extreme case, where diffusivities of the population *A* and *B* were 1×10^{-12} and 4×10^{-12} m^2 s^{-1}, respectively, population *B* in the *trans* was almost 1000 times more than population *A* in the *trans*. These results show that the nanofluidic molecular CCD can sensitively separate DNA molecules based on their diffusivities.

3.6. Impact of gating set numbers on separation performance

To evaluate the effect of the number of gating sets on the separation performance, we studied the separation of two DNA subpopulations with different diffusivities (2×10^{-12} and 3×10^{-12} m^2 s^{-1}) through the nanofluidic CCD with a different number of sets (1–6). The gating voltage was fixed at 1.2 V with a frequency of 0.1 Hz. Since the nanochannel length increases as we increase the number of sets, we scaled up the voltage across the channel to make the transverse electric field constant. Figure 5(a) presents the transfer efficiencies of the two populations through the nanofluidic molecular CCD with a different number of sets over 1000 s (100 cycles). As shown, increasing the number of sets would decrease the transfer efficiency in a fixed time frame. This is not surprising since as the number of sets is increased, the channel length would be increased, and consequently, more time is required to transfer the molecules to the *trans*.

Figure 5(b) presents the RA of the two populations for the different numbers of sets. For all cases, after an initial increase, RA declines over time. Eventually, after two populations were completely transferred to the *trans,* RA will become 1. However, as we increase the number of sets, the rate of decline is lower, which means the separation becomes less operation time-sensitive. This is because the transfer of the molecules through the nanochannel occurs at a lower rate as we increase the number of sets. For instance, in the case of 1 set, after 1000 s both populations of the molecules were transferred to the *trans*, and consequently, the RA became 1 (no separation anymore). These results suggest that while increasing the number of sets would decrease the transfer efficiency; it would improve the separation stability (less operation time-sensitive).

4. Conclusions

In summary, we presented the nanofluidic charged-coupled device and evaluated its performance towards controlled DNA transport and separation. This study aims to provide useful and practical insight to establish the design parameters

for the nanofluidic charged-coupled devices. We developed a device model to explore the effect of surface charge, gating voltage and frequency, molecules diffusivity, and the number of gate sets on the transport and separation efficiency. The result of the surface charge effect on the transfer efficiency revealed that increasing the negative surface charge magnitude would decline the transfer efficiency. We found that increasing the gating voltage and diffusivity of the molecules enhances the transfer efficiency of the nanofluidic CCD. We also found that the optimized transfer efficiency occurs when the clocking period matches the time required for the molecules to diffuse to the next electrode ($1/f \sim L_G^2/D$). We demonstrated that nanofluidic CCD could separate two populations based on their diffusivities. Although the results presented in this work were computed using DNA electrophoretic mobility and diffusivity, the principle could be well extended to other charged biomolecules such as RNAs and proteins. In this study, we only consider one dimension of gates in our simulations. However, a 2D array of gates could be the next step for the nanofluidic CCD design, giving us more options for molecule manipulation. While the fabrication of a prototype device and experimental realization is crucial for exploring the nanofluidic CCD, we anticipate these findings would provide insight into the future design of molecular CCD and biomolecular transport and separation.

Acknowledgments

This work supported by the National Science Foundation under Grant No. 1710831. Any opinions, findings, and conclusions or recommendations expressed in this work are those of the authors and do not necessarily reflect the views of the National Science Foundation.

Data availability statement

The data that support the findings of this study are available upon reasonable request from the authors.

ORCID iDs

Weihua Guan https://orcid.org/0000-0002-8435-9672

References

[1] Sparreboom W, van den Berg A and Eijkel J C T 2009 Principles and applications of nanofluidic transport *Nat. Nanotechnol.* **4** 713–20
[2] Bocquet L 2020 Nanofluidics coming of age *Nat. Mater.* **19** 254–6
[3] Liang S, Xiang F, Tang Z, Nouri R, He X, Dong M and Guan W 2020 Noise in nanopore sensors: sources, models, reduction, and benchmarking *Nanotechnol. Precis. Eng.* **3** 9–17
[4] Bohn P W 2009 Nanoscale control and manipulation of molecular transport in chemical analysis *Annu. Rev. Anal. Chem.* **2** 279–96
[5] Radha B, Esfandiar A, Wang F, Rooney A, Gopinadhan K, Keerthi A, Mishchenko A, Janardanan A, Blake P and Fumagalli L 2016 Molecular transport through capillaries made with atomic-scale precision *Nature* **538** 222–5
[6] Cheng L J and Guo L J 2010 Nanofluidic diodes *Chem. Soc. Rev.* **39** 923–38
[7] Ali M, Ramirez P, Nasir S, Cervera J, Mafe S and Ensinger W 2019 Ionic circuitry with nanofluidic diodes *Soft Matter* **15** 9682–9
[8] Guan W, Fan R and Reed M A 2011 Field-effect reconfigurable nanofluidic ionic diodes *Nat. Commun.* **2** 506
[9] Tybrandt K, Forchheimer R and Berggren M 2012 Logic gates based on ion transistors *Nat. Commun.* **3** 1–6
[10] Gabrielsson E O, Tybrandt K and Berggren M 2014 Polyphosphonium-based ion bipolar junction transistors *Biomicrofluidics* **8** 064116
[11] Gajar S A and Geis M W 1992 An ionic liquid-channel field-effect transistor *J. Electrochem. Soc.* **139** 2833–40
[12] Karnik R, Fan R, Yue M, Li D Y, Yang P D and Majumdar A 2005 Electrostatic control of ions and molecules in nanofluidic transistors *Nano Lett.* **5** 943–8
[13] Fan R, Yue M, Karnik R, Majumdar A and Yang P D 2005 Polarity switching and transient responses in single nanotube nanofluidic transistors *Phys. Rev. Lett.* **95** 086607
[14] Karnik R, Castelino K and Majumdar A 2006 Field-effect control of protein transport in a nanofluidic transistor circuit *Appl. Phys. Lett.* **88** 123114
[15] Fan R, Huh S, Yan R, Arnold J and Yang P D 2008 Gated proton transport in aligned mesoporous silica films *Nat. Mater.* **7** 303–7
[16] Nam S W, Rooks M J, Kim K B and Rossnagel S M 2009 Ionic field effect transistors with sub-10 nm multiple nanopores *Nano Lett.* **9** 2044–8
[17] Joshi P, Smolyanitsky A, Petrossian L, Goryll M, Saraniti M and Thornton T J 2010 Field effect modulation of ionic conductance of cylindrical silicon-on-insulator nanopore array *J. Appl. Phys.* **107** 054701
[18] Liu Y and Yobas L 2016 Slowing DNA translocation in a nanofluidic field-effect transistor *ACS Nano* **10** 3985–94
[19] Singh K P and Guo C 2017 Current–voltage characteristics influenced by the nanochannel diameter and surface charge density in a fluidic field-effect-transistor *Phys. Chem. Chem. Phys.* **19** 15701–8
[20] Guo W, Cao L, Xia J, Nie F Q, Ma W, Xue J, Song Y, Zhu D, Wang Y and Jiang L 2010 Energy harvesting with single-ion-selective nanopores: a concentration-gradient-driven nanofluidic power source *Adv. Funct. Mater.* **20** 1339–44
[21] Zhu G, Lin Z-H, Jing Q, Bai P, Pan C, Yang Y, Zhou Y and Wang Z L 2013 Toward large-scale energy harvesting by a nanoparticle-enhanced triboelectric nanogenerator *Nano Lett.* **13** 847–53
[22] Xie Y B, Bos D, van der Meulen M J, Versluis M, van den Berg A and Eijkel J C T 2016 Ballistic energy conversion: physical modeling and optical characterization *Nano Energy* **30** 252–9
[23] Guan W, Li S X and Reed M A 2014 Voltage gated ion and molecule transport in engineered nanochannels: theory, fabrication and applications *Nanotechnology* **25** 122001
[24] Kim B, Heo J, Kwon H J, Cho S J, Han J, Kim S J and Lim G 2013 Tunable ionic transport for a triangular nanochannel in a polymeric nanofluidic system *ACS Nano* **7** 740–7
[25] Fuest M, Rangharajan K K, Boone C, Conlisk A and Prakash S 2017 Cation dependent surface charge regulation in gated nanofluidic devices *Anal. Chem.* **89** 1593–601

[26] Mádai E, Matejczyk B, Dallos A, Valiskó M and Boda D 2018 Controlling ion transport through nanopores: modeling transistor behavior *Phys. Chem. Chem. Phys.* **20** 24156–67
[27] Kurulugama R T, Nachtigall F M, Lee S, Valentine S J and Clemmer D E 2011 Overtone mobility spectrometry: I. Experimental observations *J. Am. Soc. Mass Spectrom.* **20** 729–37
[28] Stern M B, Geis M W and Curtin J E 1997 Nanochannel fabrication for chemical sensors *J. Vac. Sci. Technol.* B **15** 2887–91
[29] Paik K-H, Liu Y, Tabard-Cossa V, Waugh M J, Huber D E, Provine J, Howe R T, Dutton R W and Davis R W 2012 Control of DNA capture by nanofluidic transistors *ACS Nano* **6** 6767–75
[30] Schasfoort R B M, Schlautmann S, Hendrikse L and van den Berg A 1999 Field-effect flow control for microfabricated fluidic networks *Science* **286** 942–5
[31] Boyle W S and Smith G E 1970 Charge coupled semiconductor devices *Bell Syst. Tech. J.* **49** 587–93
[32] Heller C 2001 Principles of DNA separation with capillary electrophoresis *Electrophoresis* **22** 629–43
[33] Viefhues M, Regtmeier J and Anselmetti D 2013 Fast and continuous-flow separation of DNA-complexes and topological DNA variants in microfluidic chip format *Analyst* **138** 186–96
[34] Nkodo A E, Garnier J M, Tinland B, Ren H, Desruisseaux C, McCormick L C, Drouin G and Slater G W 2001 Diffusion coefficient of DNA molecules during free solution electrophoresis *Electrophoresis* **22** 2424–32
[35] Yeh L-H, Xue S, Joo S W, Qian S and Hsu J-P 2012 Field effect control of surface charge property and electroosmotic flow in nanofluidics *J. Phys. Chem.* C **116** 4209–16
[36] Prakash S and Conlisk A 2016 Field effect nanofluidics *Lab Chip* **16** 3855–65
[37] Xing X, Ma W, Zhao X, Wang J, Yao L, Jiang X and Wu Z 2018 Interaction between surface charge-modified gold nanoparticles and phospholipid membranes *Langmuir* **34** 12583–9
[38] Daiguji H, Oka Y and Shirono K 2005 Nanofluidic diode and bipolar transistor *Nano Lett.* **5** 2274–80
[39] Guan W and Reed M A 2012 Electric field modulation of the membrane potential in solid-state ion channels *Nano Lett.* **12** 6441–7
[40] Bhattacharjee S, Mondal M and De S 2017 Effects of overlapping electric double layer on mass transport of a macro-solute across porous wall of a micro/nanochannel for power law fluid *Electrophoresis* **38** 1301–9